Neurobiology of Disease 201 (2024) 106668

Contents lists available at ScienceDirect

Neurobiology of Disease

journal homepage: www.elsevier.com/locate/ynbdi

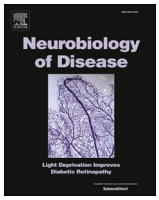

General loss of proteostasis links Huntington disease to Cockayne syndrome

Maximilian Wagner [a,d], Gaojie Zhu [a], Fatima Khalid [a], Tamara Phan [a], Pallab Maity [a], Ludmila Lupu [a], Eric Agyeman-Duah [b], Sebastian Wiese [c], Katrin S. Lindenberg [d], Michael Schön [e], G. Bernhard Landwehrmeyer [d], Marianna Penzo [f], Stefan Kochanek [g], Karin Scharffetter-Kochanek [a], Medhanie Mulaw [b,*], Sebastian Iben [a,*]

[a] Department of Dermatology and Allergic Diseases, University of Ulm, James-Franck Ring N27, 89081 Ulm, Germany
[b] Unit for Single-Cell Genomics, Medical Faculty, University of Ulm, James-Franck Ring N27, 89081 Ulm, Germany
[c] Core Unit Mass Spectrometry, University of Ulm, Albert-Einstein Allee 11, 89081 Ulm, Germany
[d] Department of Neurology, University of Ulm, Oberer Eselsberg 45, 89081 Ulm, Germany
[e] Department of Anatomy, University of Ulm, Albert-Einstein Allee 11, 89081 Ulm, Germany
[f] Department of Medical and Surgical Sciences and Center for Applied Biomedical Research (CRBA), University of Bologna, Via Massarenti 9, 40138 Bologna, Italy
[g] Department of Gene Therapy, University of Ulm, Helmholtzstraße 8/1, 89081 Ulm, Germany

ARTICLE INFO

Keywords:
Huntington disease
Cockayne syndrome
Ribosome
Loss of proteostasis
Protein carbonylation

ABSTRACT

Cockayne syndrome (CS) is an autosomal recessive disorder of developmental delay, multiple organ system degeneration and signs of premature ageing. We show here, using the RNA-seq data from two CS mutant cell lines, that the CS key transcriptional signature displays significant enrichment of neurodegeneration terms, including genes relevant in Huntington disease (HD). By using deep learning approaches and two published RNA-Seq datasets, the CS transcriptional signature highly significantly classified and predicted HD and control samples. Neurodegeneration is one hallmark of CS disease, and fibroblasts from CS patients with different causative mutations display disturbed ribosomal biogenesis and a consecutive loss of protein homeostasis - proteostasis. Encouraged by the transcriptomic data, we asked whether this pathomechanism is also active in HD. In different HD cell-culture models, we showed that mutant Huntingtin impacts ribosomal biogenesis and function. This led to an error-prone protein synthesis and, as shown in different mouse models and human tissue, whole proteome instability, and a general loss of proteostasis.

1. Introduction

Because ageing is the single most important risk factor for disease development, insights into the mechanisms of ageing may yield strategies to prevent or treat ageing-associated diseases. Ageing can be studied in progerias, genetically defined syndromes that display accelerated ageing in different organ systems. Cockayne syndrome (CS) is a degenerative childhood disorder with premature symptoms and signs of ageing like cataract formation, loss of subcutaneous fat, alopecia and severe cachexia frequently leading to early mortality (Laugel, 1993). Neurodegenerative features include de- and dysmyelination and basal ganglia calcification (Karikkineth et al., 2017), and can be accompanied by lipofuscin accumulation (Levin et al., 1983). Huntington disease (HD), by contrast, is a dominantly inherited disorder, typically of adult-onset, caused by a dynamic CAG repeat expansion mutation in the Huntingtin-(HTT)-gene, resulting in a prolongation of a polyglutamine stretch in HTT. Degeneration of the striatum and cortical involvement lead to a progressive movement disorder and cognitive decline together with behavioural alterations and unintended weight loss with sarcopenia (Jurcau, 2022; Bates et al., 2015; Tabrizi et al., 2020). Childhood degeneration indicates that the underlying pathomechanisms are so dominant, that they overwhelm cellular and organismal compensation mechanisms. Adult or late-onset degeneration suggests that the pathomechanisms only reach the disease threshold when cellular and organismal compensation mechanisms decrease. The exact nature of the pathomechanisms in HD is a matter of debate (Jurcau, 2022) and, asking whether the recently described loss of proteostasis in CS (Alupei et al., 2018) is a feature in other neurodegenerative diseases, we here describe a novel facet of the pathophysiology of HD. CS can be provoked by mutations in DNA-repair genes; however, because a failure in DNA-

* Corresponding authors at: James-Franck Ring N27, 89081 Ulm, Germany.
E-mail addresses: medhanie.mulaw@uni-ulm.de (M. Mulaw), sebastian.iben@uni-ulm.de (S. Iben).

https://doi.org/10.1016/j.nbd.2024.106668
Received 29 April 2024; Received in revised form 13 August 2024; Accepted 13 September 2024
Available online 14 September 2024

repair does not sufficiently explain the neurodegenerative phenotype (Brooks, 2013), others and we demonstrated that the CS gene products are all involved in ribosomal biogenesis (Iben et al., 2002; Bradsher et al., 2002; Koch et al., 2014; Lanzafame et al., 2021). CS mutations affect ribosomal biogenesis and maturation, protein synthesis and proteome stability, thereby inducing a loss of proteostasis (Alupei et al., 2018; Lebedev et al., 2008; Qiang et al., 2021). Because the loss of proteostasis is a hallmark of adult-onset neurodegeneration, we hypothesise that disturbances in ribosomal biogenesis and performance might contribute to neurodegeneration in HD. In this study, we provide mechanistic insights into the cellular pathology of HD and identify ribosomal biogenesis and function as essential and susceptible cellular pathways to maintain general cellular proteostasis.

2. Results

We recently generated an RNA-Seq data set of Cockayne patient-derived fibroblast cell lines with causative mutations in the Cockayne

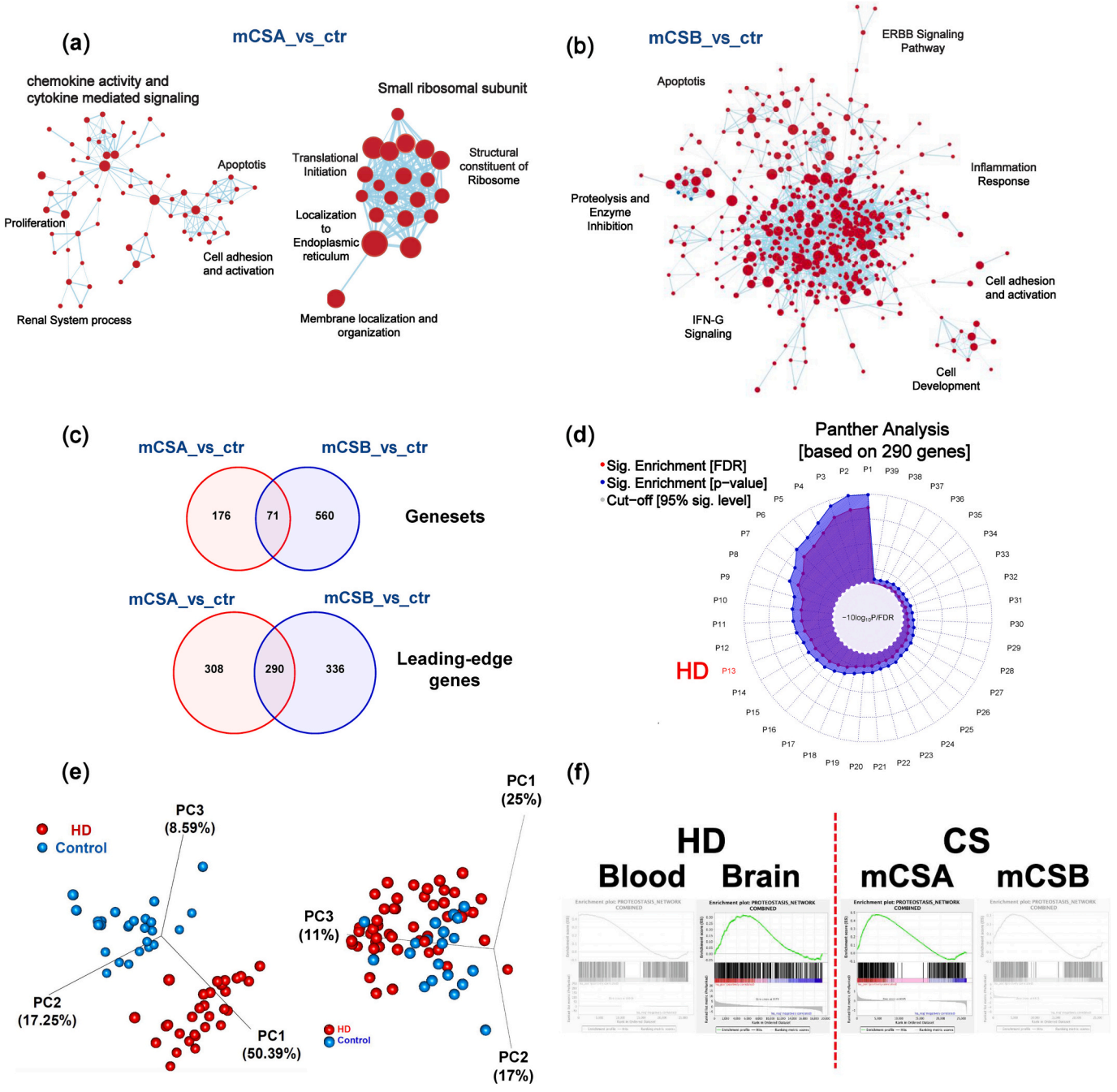

Fig. 1. Transcriptomic analysis identified HD as a CS-related disease. a. Gene Set Enrichment (GSEA)-based network map of significant gene sets in mCSA. Two core networks were identified: chemokine- and apoptosis-related processes and ribosomal translation and localisation. b. Mutant CSB enrichment analysis yielded significant terms related to inflammation, IFN signalling and proteolysis. c. Overlap between significant gene sets (upper panel) and leading-edge genes (lower panel) between mCSA and mCSB as compared to their respective controls. d. Protein annotation through evolutionary relationship (Panther) analysis of the leading-edge genes yielded 39 significant terms. e. PCA based on the 290 genes also revealed segregation between HD and control samples (left) that was not accomplished with 290 random genes (right). f. Proteostasis-related genes were tested in CS and HD samples in our current study. Of the four datasets, brain-derived HD samples and mCSA mutant cell line (CS) showed statistically significant enrichment.

syndrome A (CSA) protein (mCSA) and Cockayne syndrome B (CSB) protein (mCSB), as well as wild-type (WT) reconstituted syngenic cells (Alupei et al., 2018). Using this dataset, we performed Gene Set Enrichment Analysis (GSEA) for each mutant and control cell line pair using the biological process (BP) Gene Ontology (GO) terms. Comparing mCSA to ctr (WTCSA), we identified 247 significantly upregulated gene sets (p-value <0.05; FalseDiscoveryRate (FDR) < 0.25; Supplementary Table 1 and Supplementary Fig. 1a). A network analysis of the significantly dysregulated gene sets identified the networks "chemokine and cytokine activity", "proliferation", "apoptosis", "cell adhesion/activation processes" (Fig. 1a; left panel and Supplementary Fig. 1c), and "structural component of the ribosome", "translational initiation" and "localization to the endoplasmic reticulum" as the major networks (Fig. 1a; right panel). In comparing mCSB to ctr (WTCSB), 631 gene sets were significantly upregulated, while 5 gene sets were significantly downregulated in the mCSB mutant cell line (Supplementary Table 2 and Supplementary Fig. 1b). The pattern was broader when compared to the mCSA results, and "apoptosis", "proteolysis" and "enzyme initiation", "interferon gamma signaling", "inflammation response" and "cell adhesion and activation" were some of the network members (Fig. 1b and Supplementary Fig. 1d) We subsequently looked at the overlap between the significant gene sets of the two comparisons and identified 71 common gene sets and 290 leading-edge genes (Fig. 1c and Supplementary Table 3). By taking the 290 leading-edge genes, we performed a Panther pathway analysis (Thomas et al., 2003) and identified 39 significantly enriched pathways (adj. p-value <0.05; Fig. 1d and Supplementary Table 5). Interestingly, neurodegenerative disease terms, including HD, Alzheimer's disease (AD) and Parkinson's disease (PD), were statistically significant in skin cells (Fig. 1d; HD is pathway number 13; P13). Subsequently, we acquired two publicly available HD datasets: an RNA-Seq dataset of HD patient monocytes (Miller et al., 2016) (accession number PRJEB12995) and an mRNA-Seq expression profiling of human post-mortem BA9 brain tissue (prefrontal cortex) of HD (Labadorf et al., 2015) (accession number GSE64810). We first performed a Principal Component Analysis (PCA) of the two public datasets using the 290 leading-edge genes. We observed that HD and control samples were segregated into distinct clusters (Fig. 1e left), indicating that the 290 leading-edge genes from CS, but not 290 random genes (Fig. 1e right), sufficiently recapitulated the distinct transcriptional profile of HD. In a GSEA analysis of reactomes related to proteostasis (translation, protein ubiquitination, chaperone-mediated autophagy and protein folding), we observed that they were significantly enriched in brain-derived HD samples and mCSA mutated CS samples (FDR and a p-value cut-off of 0.25 and 0.05, respectively) (Fig. 1f). More importantly, using deep learning models, we demonstrated that CS common leading-edge genes could classify and predict group membership of HD and control samples in a tissue-independent manner. These findings encouraged us to hypothesise that related pathomechanisms play a role in both, HD and CS. In CS, we previously identified disturbances in ribosomal biogenesis and function as a pathomechanism leading to a general loss of proteostasis (Alupei et al., 2018). HD is caused by a CAG-triplet repeat expansion in exon1 of the *HTT*-gene, resulting in an elongated polyglutamine (Q) stretch in the N-terminus of the protein HTT. We now used lymphoblastoid cells from two HD patients with different lengths of the polyglutamine (Q) repeat of 46 and 93, respectively, and two controls with a repeat length of Q17 (HTT western blot in Fig. 2a and Supplementary Fig. 7). We first tested whether HTT binds the ribosomal DNA (rDNA) coding for the functional backbone of the

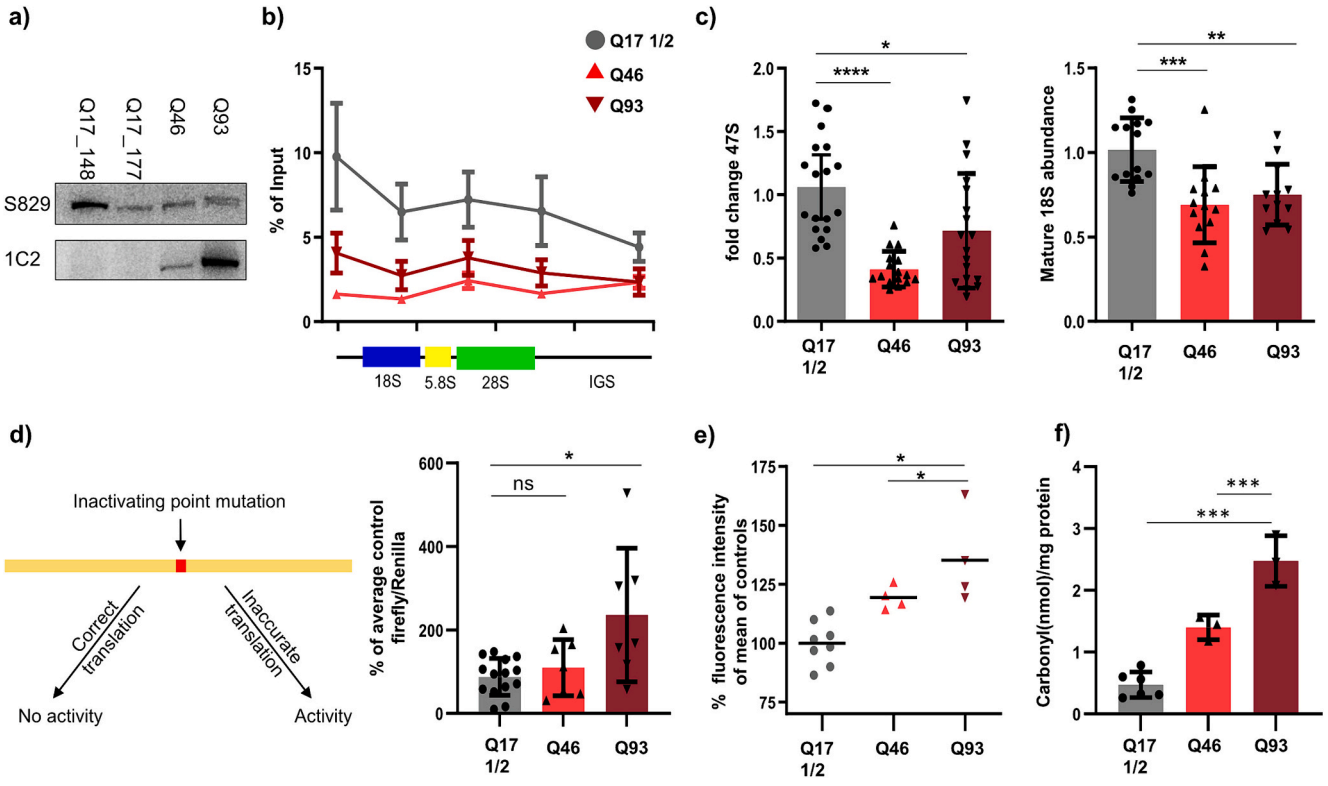

Fig. 2. Huntingtin binds rDNA and mutation influences rRNA synthesis and ribosomal performance. a. Western blot analysis of HTT with anti HTT antibody clone S829. mHTT was detected by anti polyQ antibody clone 1C2 in lysates of lymphoblastoid cell lines. b. Chromatin immunoprecipitation analysis of HTT binding to different regions of rDNA in control (grey) and HD patient (orange, red) lymphoblastoid cells. $n = 3$–4. c. Relative quantification of the 47S pre-rRNA precursor and mature 18S rRNA by qPCR. $n = 14$. d. Translational fidelity assay assessing the translational error rate of HD patient cells in a luciferase-based transfection experiment. $n = 6$. e. 4,4′-dianilino-1,1′-binaphthyl-5,5′-disulfonic acid (BisANS)-labelling of hydrophobic side chains after partial unfolding with 2 M urea. $n = 4$. f. Protein carbonylation determined using the Carbonylation Assay Kit. $n = 3$. (For interpretation of the references to colour in this figure legend, the reader is referred to the web version of this article.)

ribosome. Chromatin-immunoprecipitation and qPCR analysis detected that HTT binds coding and non-coding regions of the rDNA (Fig. 2b) and that it binds to gene-internal regions (H8) weakly when the polyglutamine stretch is expanded (Supplementary Fig. 2a). qPCR analysis of rRNA expression showed a reduction of 47S pre-rRNA transcription, indicating a reduced or repressed initiation of RNA polymerase I transcription as well as a lower abundance of the mature 18S rRNA, the backbone of the small ribosomal subunit, in HD cells (Fig. 2c). This pattern resembles the ribosome biogenesis alterations described in CS cells (Alupei et al., 2018; Qiang et al., 2021). Moreover, northern blot analyses revealed an accumulation of immature processing intermediates in HD cells (Supplementary Fig. 2b) as recently described by Sönmez et al. (Sönmez et al., 2021), indicating an rRNA maturation defect in HD, like in CS. Because alterations in ribosomal biogenesis in CS can result in dysfunctional ribosomes (Alupei et al., 2018; Qiang et al., 2021), we subsequently assessed the error-rate of the translation process. A mutant luciferase reporter plasmid with a point mutation (K529N), inactivating luciferase activity, was transfected in the lymphoblastoid control and HD cells (Fig. 2d). We observed a re-activation of luciferase in the Q93 cells, indicating an error-prone translation process. Challenging the proteome with unfolding stress by urea led to an increased exposure of hydrophobic side chains in HD cells (Fig. 2e), indicating an unstable proteome. Moreover, there was increased protein carbonylation of the proteome detectable in HD cells (Fig. 2f), presumably a consequence of translational errors (Dukan et al., 2000), because no elevated reactive oxygen species (ROS) were detected (Supplementary Fig. 3). Translational infidelity and downstream events were mild in the Q46 patient lymphoblasts, but because there is a reported somatic repeat instability in neurons that leads to a brain-specific amplification of the polyglutamine stretch in HTT (Kennedy, 2003), these parameters might be of relevance for HD development. We took advantage of a doxycycline-inducible HTT-expression system in HEK (human embryonic kidney) cells expressing either WT (HTT17) or mutant (HTT128) HTT, showing that induction of the mutant, but not WT HTT, provoked an error-prone translation process at the ribosome (Fig. 3a), accompanied by an elevated protein carbonylation (Fig. 3b). These experiments suggested that in HD, like in CS, perturbations of ribosomal biogenesis lead to a decline in the quality of overall protein synthesis. Investigating several mouse models of HD, we first stained aggregated HTT and found a high aggregation load in brains of symptomatic R6/2 mice in contrast to the mildy affected HdhQ111 mice (Fig. 3c).Subsequently, we stained for carbonylated proteins and observed strong reactivity in sick 12-week-old R6/2 mice but not in HDHQ111 mice (1 year) (Fig. 3d). Subsequently, we tested the aggregation properties of the proteome of three different mouse models by applying a short heat shock or sequential heat treatment (Treaster et al., 2014) and observed a significantly elevated aggregation propensity of proteins extracted from two different symptomatic HD mouse models (R6/2 12 weeks; ZQ175 het 9 months), but not from the asymptomatic mouse model (HDHQ111 hom, 1 year) (Fig. 3e, Supplementary Fig. 4), again resembling the general proteomic instability found in CS (Qiang et al., 2021). Analysing protein carbonylation in the striata of ZQ175 mice revealed highly significant elevation of carbonylated proteins (Fig. 3f). Finally, having access to human post-mortem brain tissue from HD patients (Table 1) (Supplementary Table 6)., we stained cortex for carbonylated proteins in areas known to be pathologically affected in HD in comparison to unaffected areas. Indeed, Brodmann area (BA) 4, where corticostriatal neurons are highly vulnerable in HD (Pressl et al., 2024), displayed a strong positive reaction for protein carbonylation in contrast to BA9 and BA17 (Fig. 3h, Supplementary Fig. 5) On the other hand all the areas were positive for HTT aggregates, suggesting that protein carbonylation but not HTT aggregates indicates affected areas (Fig. 3g, Supplementary Fig. 6). Taken together, our data support the hypothesis that HD is accompanied, if not caused, by a general loss of proteostasis by the ribosome as already shown for CS.

3. Discussion

In this study, we elucidated that impaired protein synthesis at the ribosome contributes to the loss of proteostasis in HD using complementary approaches when comparing a model disease of ageing characterised by neurodegeneration with HD.

Identifying common transcriptional programmes or signatures between various neurological disorders is a long-standing aim We propose that general mechanisms of neurodegeneration can be elucidated by identifying overlaps between distinct disorders. Sagar et al. (Sagar et al., 2017) identified convergent gene networks in seven major neurological disorders: AD, PD, multiple sclerosis, age macular degeneration, ALS vascular dementia and restless leg syndrome. Noori et al. (Noori et al., 2021a) also performed a meta-analysis of transcriptomics of AD, Lewy body diseases (LBD) and amyotrophic lateral sclerosis and frontotemporal dementia (ALS-FTD) to identify common/shared gene networks. In a follow-up study, Noori et al. (Noori et al., 2021b) performed a systematic meta-analysis of 60 human central nervous system transcriptomic datasets (2600 in total) including of AD, LBD and ALS-FTD patients. Arneson et al. (Arneson et al., 2018) investigated AD, PD and amyotrophic lateral sclerosis to identify shared mechanisms among neurodegenerative diseases, including genetic factors and gene networks. Mukherjee et al. (Mukherjee et al., 2019), when considering AD, PD and HD and employing weighted gene co-expression network analysis, identified a preserved network of immune/microglia genes among the entities. CS transcriptomic datasets are not as readily or extensively available as for HD. This indeed limits the application of methodologies that take advantage of large-scale studies. Okur et al. (Okur et al., 2020), in cross-species transcriptomic analysis, identified DNA damage accumulation, mitochondrial dysfunction and compromised mitophagy/autophagy as interconnected processes contributing to accelerated ageing. Furthermore, they indicated that CSA and CSB proteins in CS use NAD+ signalling to maintain mitochondrial homeostasis. Moreover, the interplay between NAD+ supplementation, mitochondria and mitophagy provides insight into the development of therapeutic strategies in the treatment of DNA repair-accelerated ageing models like CS. Our observation regarding the significantly higher impact of CSB on the transcriptome and biological processes (see results section and Fig. 1) is in agreement with Wang et al. (Wang et al., 2014) who showed that, even in the absence of DNA damage, CSB affects the expression of thousands of genes. It has also been reported that dysregulation of the insulin-like growth factor-1 pathway, synapse formation and maintenance and neuronal differentiation are deregulated in CSB neurons (Vessoni et al., 2016). More recently, Liang et al. (Liang et al., 2023), using an RNA-Seq approach in multiple cell types, identified necdin as a target of the CSB protein.

In the current study, we demonstrated a novel link between CS and HD by combining various bioinformatic approaches, including GSEA, top scoring pairs, support vector machines and deep learning algorithms. We showed that 290 core leading-edge genes shared between two CS mutant cell lines are not only strongly correlated but are sufficient to identify HD samples. Furthermore, we observed that proteostasis-related genes are significantly enriched in both CS and HD samples. This is in agreement with the aforementioned report by Noori et al. (Noori et al., 2021b), where their meta-analysis revealed neuroinflammation, deficient energy metabolism and proteostasis failure as a common phenomenon across neurodegeneration.

The high level of consistency between patient samples of different origins argues in favour of the assumption that we identified general cellular mechanisms that play a role in all assessed cell types and tissues. This hypothesis is supported by the fact that HTT is globally, if not ubiquitously, expressed (Laugel, 1993; Strong et al., 1993; Li et al., 1993; Landwehrmeyer et al., 1995), indicating that it interferes with and mediates general cellular pathways. Accordingly, mHTT might disturb these general pathways in different cells; however, only specific cells might be vulnerable to and affected by these disturbances. Moreover,

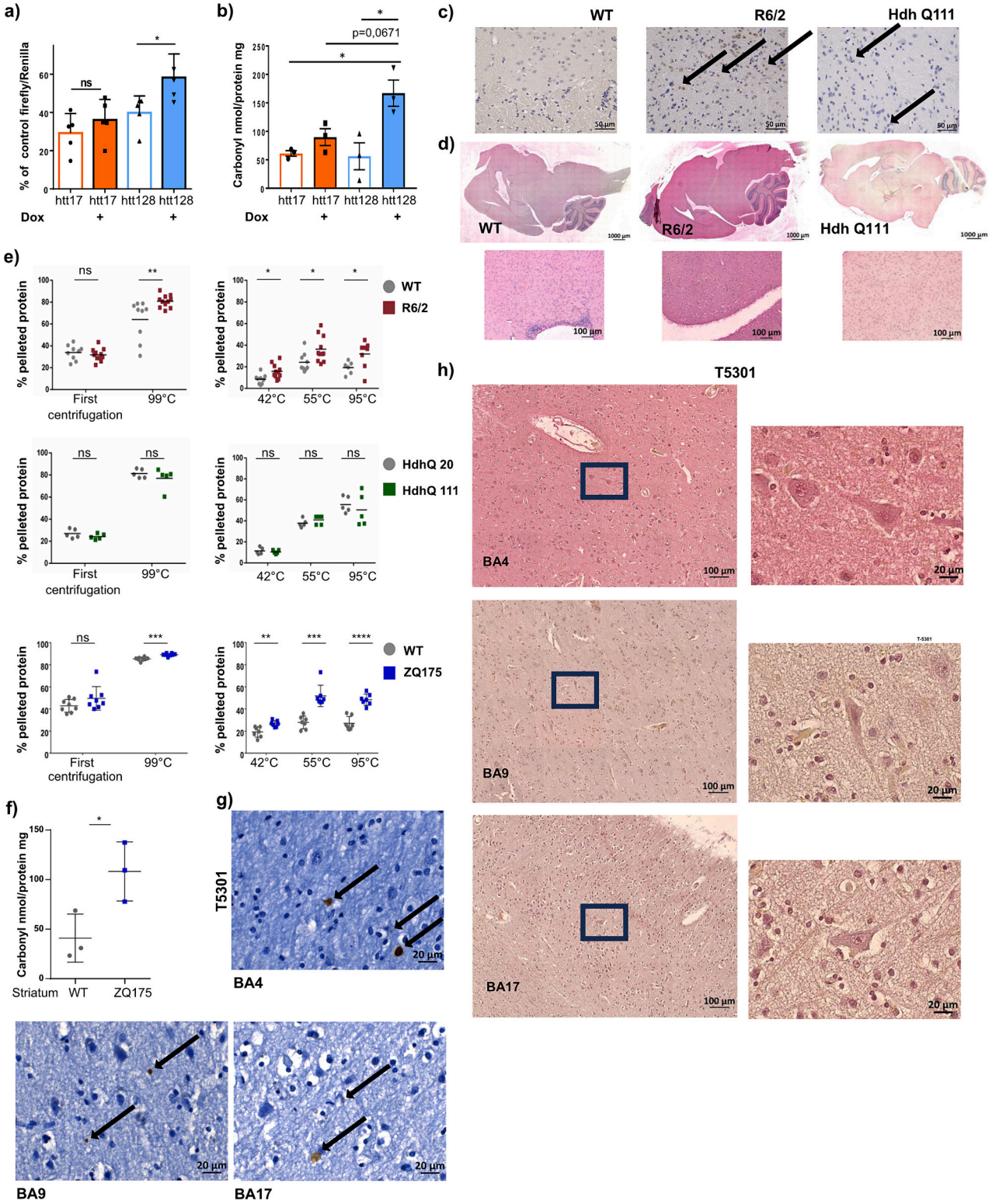

Fig. 3. Elevated ribosomal error-rate, protein carbonylation and aggregation in HD-models and human tissue. a. Ribosomal error-rate in an inducible Huntingtin expression system. n = 4. b. Quantification of protein carbonylation by DNPH labelling. n = 3. c. Anti HTT aggregate staining with anti-HTT antibody clone EM48 in brain sections of HD mouse models; representative images are shown. d. Protein carbonylation in brain sections of HD mouse models (overview/striatum). n = 3, representative images are shown. e. Proteome stability test by short heat treatments and centrifugation. Cytoplasmic extracts from WT and R6/2 (top; $n = 8–11$), respective HDHQ20 and HDHQ111 (middle; $n = 5$) and ZQ175 het and WT (bottom; $n = 7–8$) mouse brains were challenged by a short heat shock (left) or stepwise treatment (right) and subsequently centrifuged and quantified. f. Quantification of protein carbonylation by DNPH labelling in striata of ZQ175 het and WT mice. n = 3. g. Anti HTT aggregate staining with anti-HTT antibody clone EM48 in brain sections of different Brodmann areas of human HD brain tissue; representative images are shown. h. Anti-DNP carbonyl staining of different Brodmann areas of human HD brain tissue Left panel shows overview in 400× magnification, black box marks location of the detail image on the right (630× magnification). n = 6, representative images are shown.

Table 1
HD cases used in this study.

T-ID	Sex	Age	Diagnosis	CAG length
4337	W	40	HD	49/17
4493	W	50	HD	47/17
4501	W	8	HD	105/22
4522	M	42	HD	52/17
4830	W	63	HD	45/12
5301	W	64	HD	46/19

brain-specific repeat instability and repeat amplification of mHTT (Lee et al., 2019) might induce neurodegeneration. One of the general pathways perturbed by mHTT appears to be ribosomal biogenesis and function. This hypothesis is based on the one hand by gene-expression analysis that implies that alterations in proteostasis, common in both diseases, might be caused by related pathomechanisms. On the other hand, we identified strikingly similar disturbances in ribosomal biogenesis and function in both CS and HD. Ribosomal dysfunction can destabilise the proteome and impact gene transcription (Tahmasebi et al., 2018). Proteostatic imbalances may affect gene expression, for example, at the level of p-eIF2alpha that represses general translation in favour of translating typical stress-related mRNAs like the transcription factors activating transcription factor (ATF)4, C/EBP homologous protein Chop and ATF5 (Back, 2020). Translation disturbances at the ribosome are already described for HD (Eshraghi et al., 2021).Eshragi et al. demonstrated a direct interaction of WT/mHTT with the translating ribosome and proposed that the detected alteration in the translatome in HD originates from this interaction. Here we add a novel facet to these insights by the identification of a physical involvement of HTT in ribosomal biogenesis. First, we identified a direct association of HTT with rDNA by chromatin immunoprecipitation (ChIP) analysis. This is in agreement with the observations of Cha and colleagues that HTT and mHTT can bind to gene promotors and influence gene expression directly and differently (Benn et al., 2008).

ChIP experiments revealed a direct attraction of HTT to rDNA and this association was reduced in the 3′ part of the rDNA when HTT is a mutant. Mutant, truncated CSB protein, responsible for 70 % of CS cases, also binds to rDNA and disrupts transcription elongation by RNA polymerase I (Lebedev et al., 2008) followed by rRNA-processing and ribosomal assembly defects (Qiang et al., 2021). Pre-rRNA processing was also affected in HD cells and might impact on the assembly and stability of the ribosomes, giving rise to a functionally compromised protein synthesis that we detected in HD patient cells and the mHTT-inducible HEK cells. Translational infidelity, typical for CS fibroblasts (Alupei et al., 2018), might also be the source of global protein misfolding revealed by BisANS in HD patient cells. Moreover, because protein oxidation is dictated by the accuracy of the ribosomes (Dukan et al., 2000; Ballesteros et al., 2001; Nyström, 2005) and that we found no elevated ROS in the HD cells (Supplementary Fig. 3), we propose that the strongly elevated carbonylation observed in HD cells and mouse and human HD-tissue is an additional indicator of ribosomal inaccuracy as demonstrated in CS cells. Brain protein aggregation properties, as tested by heat treatment of HD mouse models, correlated with disease severity, indicating that total proteome stability was affected in these models. Aggregation stability of the proteome against stress is a feature of the longest-living animal, *Arctica islandica* (Treaster et al., 2014), and proteome stability evolved with a prolonged lifespan as also shown for the naked mole rat *Heterocephalus glaber* (Azpurua et al., 2013). It is conceivable that exacerbated proteome instability may predispose to cellular dysfunction, particularly in vulnerable cell types. Moreover, the observed loss of proteostasis in HD affected a significant proportion of the proteome as shown by the BisANS, carbonylation and aggregation assays. These results argue against the concept that cellular dysfunction in HD results primarily from an accumulation of selectively misfolded HTT, rather from a more general misfolding problem likely as a consequence of translational infidelity of the ribosome. This hypothesis is supported by the observations that polyQ expression impacted the aggregation properties of unrelated proteins (Gidalevitz et al., 2006).

Taken together, the interesting transcriptomics-based association between CS and HD provides evidence that neurodegenerative diseases might share common cellular programmes than can be deciphered using large scale -omics datasets. Such datasets, coupled with state-of-the-art analysis like machine learning, will not only provide novel insights into overlapping pathomechanisms, but will also help in the development of simple but novel diagnostic and prognostic markers of neurodegenerative diseases. Finally, we here propose a novel hypothesis underlying the loss of proteostasis in HD: ribosomal biogenesis defects that impact proteome stability. Proteostasis is sustained by the balance of protein synthesis, maintenance and degradation and it is already established that mHTT affects protein synthesis by direct binding to the ribosome (Eshraghi et al., 2021). Whether the levated error-rate of the translation process is due to a physical interference of mHTT with the ribosome (gain of function) or a consequence of ribosomal biogenesis disturbances (loss of function) awaits further analysis. We here specify a general loss of proteostasis that is not confined to mHTT, rather affects the entire proteome. Employing bioinformatic transcriptomic analysis and biochemical/molecular biology techniques, we describe that – although apparently unrelated – a profoundly similar mechanism provokes the loss of proteostasis in both, HD and CS. This implies that there are general pathomechanisms in action in neurodegeneration.

3.1. *Strengths and limitations*

Strengths: First, the transcriptomic pattern of skin fibroblasts from CS classified mononuclear cells and brain areas of HD, indicating that we had identified general, systemic mechanisms that are evident in all cells but might be of pathophysiological relevance only in particular cells and tissue. Moreover, we described that a general loss of proteostasis in HD was due to an elevated protein synthesis error rate in contrast to the prevailing hypothesis that HD is characterised by a specific loss of proteostasis. One limitation of the study is that we are still unable to measure random amino-acid exchanges by mass spectrometry or related methods.

4. Conclusions

Our study demonstrated that transcriptomic analyses and biochemical verification can be applied to identify general mechanisms of pathogenesis. Moreover, the striking similarity of the disturbances in ribosomal biogenesis and function and the cellular outcomes between CS and HD suggested that common pathogenetic motifs are indeed involved, arguing in favour of the assumption that proteinopathies are characterised by similar/general disease pathways. This study also evaluated efforts to identify pathomechanisms in rare genetic model diseases that might represent general disease pathways in their extremes. One could hypothesise that a loss of proteostasis by the ribosome might also contribute to other neurodegenerative disorders.

5. Material and methods

5.1. *RNA-Seq analysis*

Data normalisation and differential expression analysis were performed using the R package limma (Ritchie et al., 2015). Heatmaps, PCA and radar plots were also generated using R (Team RC, 2015). GSEA was performed using the standalone GSEA java application (Subramanian et al., 2005; Mootha et al., 2003). An R implementation of the Keras/TensorFlow (Abadi et al., 2016) binary classifier was used for the deep learning analysis. Glorot uniform initializer and hyperbolic tangent activation were used for kernel initialisation and activation, respectively. Furthermore, stochastic gradient descent as used as a model

optimiser and binary cross-entropy for loss measurement. An initial layer of 16 units with an additional three hidden layers of 16 units was employed, with a final one output layer.

5.2. Cell culture

Cell line	characteristics
Q17_148	Immortalised lymphoblastoid cells from healthy control with 17/17 CAGs in *HTT*; EHDN 148–873-196
Q17_177	Immortalised lymphoblastoid cells from healthy control with 17/16 CAGs in *HTT*; EHDN 177–383-529
Q46	Immortalised lymphoblastoid cells from HD patient with 46/17 CAGs in *HTT*; EHDN 078–311-491
Q93	Immortalised lymphoblastoid cells from HD patient with 93/23 CAGs in *HTT*; EHDN 155–672-513
HEK Q17	see (Huang et al., 2015)
HEK Q128	see (Huang et al., 2015)

Lymphoblastoid cells from HD patients and from healthy controls were obtained from the European Huntington Disease Network (EHDN) Biorepository.

Cell culture work was performed under sterile conditions in a laminar flow hood to avoid contamination. Cells were cultured in RPMI-1640 medium containing glutamine supplemented with 20 % foetal calf serum as well as 100 U/ml penicillin and 100 U/ml streptomycin at 37 °C under 5 % CO_2.

Frozen cells were thawed rapidly at 37 °C, diluted in 9 ml pre-warmed media and pelleted by centrifugation for 5 min at 1300 rpm. Cells were resuspended with pre-warmed medium and plated into T75 flasks. Every 2–3 days the cell density was observed via a microscope and cells were sub-cultured when attaining 70 % density to maintain viability.

5.3. Mouse brain protein extracts

To prepare cytoplasmic extracts of mouse brain, frozen cortices of 12-week-old (R6/2 and WT littermates), 1-year-old (HdhQ20/111) and 9-month-old (ZQ175 and WT littermates) mice were used (. The brains were thawed, washed briefly in phosphate-buffered saline (PBS) and were individually placed within a liquid nitrogen-precooled mortar. The brain tissue was frozen again with liquid nitrogen and ground until a homogeneous powder was obtained. The powder was collected and placed in a new 1.5 ml reaction tube. The tubes were stored in liquid nitrogen until further use. Subsequently, the frozen brain powder was centrifuged for 5 min at 1700 rpm and 4 °C and the packed cell volume was determined. If the packed cell volume was <150 µl, two samples were pooled. Tissue powders were suspended in two volumes of Dignam A (containing 1 mM dithiothreitol (DTT) + complete proteinase inhibitor mix 1:50) and incubated for 10 min on ice. Afterwards, samples were pottered with a Ø60 µm syringe 25 times and centrifuged for 5 min at 5000 rpm and 4 °C. The supernatant containing the cytoplasm was transferred into a new 1.5 ml reaction tube and directly used for subsequent analysis. Pellets containing nuclei as well as extracellular matrix were stored at −80 °C.

5.4. Cytoplasmic extracts

To obtain cytoplasmic extracts of the lymphoblastoid cell lines, 4 × 10^6 cells were pelleted and resuspended in 1.5 volumes of Dignam A (including 1:50 complete protease inhibitor, 1 mM DTT). After a 10-min incubation on ice, cells were lysed by 50 strokes through a 23G syringe and centrifuged for 20 min at 10,400 *g* and 4 °C. Supernatant containing the cytoplasmic extracts was separated from the pellet containing nuclei. Cytoplasmic extracts were directly used for further analysis.

5.5. Heat sensitivity assay

The heat sensitivity assay was performed according to the method of Treaster et al. (Treaster et al., 2014). Cytoplasmic protein extracts of 100 µl from mouse brain/cell culture were subjected to ultracentrifugation (TLA-100 S/N 07 U1825, Optima MAX-XP Ultracentrifuge) for 1 h at 100,000 *g* and 4 °C. The insoluble protein pellet was resuspended in 4 M urea and the protein content respectively in the purely soluble supernatant and resolved pellet were quantified by the Bradford assay. Subsequently, the supernatants were divided for two different approaches. In the first approach, 100 µg of purely soluble supernatant were heated at 99 °C for 15 min and subsequently centrifuged for 5 min at 14,000 *g*. Finally, the amount of protein in the pellet and supernatant were quantified as before. In the second approach, 500 µg of purely soluble supernatant were heated at 42 °C for 1 h followed by ultracentrifugation for 1 h at 100,000 *g* and 4 °C. Subsequently, the protein content in the supernatant and pellet were quantified as before. Soluble supernatant from the second ultracentrifugation was further heated at 55 °C for 1 h and subjected to ultracentrifugation. Following protein quantification of the resulting pellet and supernatant, the supernatant was again heated at 95 °C for 1 h. After ultracentrifugation, the protein contents were quantified as described above.

Dignam A buffer	10 mM KCl, 10 mM Tris pH 7.9, 1.5 mM $MgCl_2$, 1:50 complete proteinase inhibitor mix, 1 mM DTT

5.6. Northern blotting

To analyse pre-rRNA processing steps, northern blot analysis was performed. A 0.9 % agarose gel was casted and equilibrated with running buffer for at least 30 min before running. Five microgrammes of total RNA from cells of interest were mixed with an equal volume of RNA loading dye (50 % formamide, 7.5 % formaldehyde, 1 × -Morpholinopropansulfonacid, 0.5 % ethidium bromide) and denatured at 65 °C for 15 min followed by cooling on ice for 5 min. The samples were loaded and the gel was run at 80 V for 3 h. Transfer of nucleic acids was performed by capillary blot, whereby a nylon membrane (RPN303S, GE Healthcare) and Whatman paper was wetted in 2 × saline sodium citrate buffer and placed on top of the RNA gel in a reservoir of 20× SSC (3 M NaCl, 0.3 M Na citrate, adjusted to pH 7). Approximately 6 cm of dry filter paper was stratified over the gel/membrane and a weight of 500 g was placed on top of this stack of paper towels. The transfer was incubated overnight. Following air drying, the membrane was crosslinked with 2× 1200 J UVC (UV Stratalinker™ 1800) and pre-hybridised with buffer (50 % formamide, 0.1 % SDS, 8× Denhards solution, 5× SSC buffer, 50 mM NaP buffer, 0.5 mg/ml t-RNA) for 2 h at 65 °C. The ^{32}P-labeled (T4 polynucleotide kinase) oligonucleotide probe was denatured at 95 °C for 10 min and added to the membrane. Following incubation for one hour at 65 °C, the membrane was hybridised at 37 °C overnight. The membrane was washed with low stringency wash buffer (2× SSC) the following day, exposed to X-ray films and quantified using Image Quant Software according to Wang et al. (2014). For rRNA processing pathway analysis, a probe binding to the region ITS1 (5′ GGGCCTCGCCCTCCGGGCTCCGTTAATGATC 3′) was used.

5.7. Carbonylation assay

The amount of carbonylated protein was determined using the Protein Carbonylation Assay Kit (Cayman Chemicals) following the manufacturer's instructions. The cells were lysed in 50 mM MES. Samples were centrifuged for 20 min at maximum speed and the supernatant was transferred into a new tube. The lysates were diluted with water to a protein content of 2 mg/ml, incubated with 2,4-dinitrophenylhydrazine (DNPH) for 1 h at room temperature and were further precipitated with 20 % trichlor-acetic acid. Following centrifugation for 10 min at 10,000

g, the pellets were washed first with 10 % TCA followed by three times with 1:1 ethanol:ethyl acetate mixture. Precipitated proteins were solubilised in 500 µl guanidine HCl (6 M), transferred into a 96-well plate and absorption was determined at an OD of 375 nm. The values were normalised to the protein content, as measured by the BCA assay. For analysis of protein carbonylation of the ZQ175 striata, frozen striata of 9-month-old ZQ175 heterozygous and WT animals were ground in a liquid nitrogen-cooled mortar. Two striata were pooled and 500 µl 50 mM MES pH 6.7 were added. Samples were homogenised with steel spheres (0.5 cm diameter) in the TissueLyser LT (Qiagen) for 10 min at 50 Hz and 4 °C. Homogenate was centrifuged for 15 min at 10,000 *g* and 4 °C. Afterwards, samples were incubated with 1 % streptomycin sulphate at room temperature for 15 min. Samples were centrifuged at 6000 ×*g* for 10 min at 4 °C. The supernatant was used to determine the protein carbonyl content as described above.

5.8. Carbonyl immunohistochemistry

Formalin-fixed paraffin-embedded brains were sectioned sagitally at 5 µm thickness.

For staining, paraffin was melted at 60 °C for 30 min and solved twice in xylene for 5 min. For rehydration, slides were placed in a descending alcohol series followed by incubation in running tap water for 30 min. Unspecific endogenous alkaline phosphatase activity was blocked using BLOXALL (Vector laboratories, SP-6000-100) for 30 min. The slides were washed for 5 min in PBS and incubated in 0.1 % DNPH for 1 h at room temperature. Following washing in PBS, a-DNP antibody (Thermo Fisher, clone LO-DNP-2) diluted 1:100 was added to the slides and incubated overnight at 4 °C in a humid chamber. After washing three times for 5 min in PBS, the slides were incubated with anti-rat biotinylated secondary antibody at a dilution of 1:50 for 30 min at room temperature. The slides were washed and incubated with ABC-AP mix (Vector laboratories, AK-5200), prepared in advance for 30 min at room temperature. After soaking for 5 min in PBS, the slides were incubated with Vector Red (Vector laboratories, SK-5100) prepared according to the manufacturer's instructions. Development was performed under microscopic control. The slides were washed for 10 min in running tap water and counterstained with haemalaun for 1 min. The slides were washed and dehydrated in an ascending alcohol series, mounted in Eukitt and analysed blinded under the microscope. Further information about HD brain sections used in this study can be found in the table below and in Supplementary Table 6.

5.9. BisANS assay

Protein folding stability was investigated using fluorescent BisANS (SIGMA) dye (Treaster et al., 2014). Cells were harvested in TNE buffer (50 mM TrisHCl, 100 Mm NaCl, 1 mM EDTA), sonicated (3 × 30 s) and centrifuged for 20 min at maximum speed (table top centrifuge). The protein concentration of the supernatant was determined by the Bradford assay. In total, 100 µg protein were subjected to 2 M urea for 2 h. BisANS was added to each sample (30 µM final concentration) and fluorescence was determined using an excitation wavelength of 375 nm and 500 nm emission.

BisANS dye	4,4′-dianilino-1, 1′-binaphthyl-5, 5′- disulphonic acid, dipotassium salt
Labelling buffer	50 mM Tris HCl, 10 mM $MgSO_4$, adjusted to PH 7.4

5.10. Transfection and luciferase assay (plasmids)

pGL3 WT-luciferase plasmid, hypoxanthine-guanine phosphoribosyltransferase (HRPT) negative control, Renilla luciferase plasmid and K529N (lysin AAA - Asn AAC) mutant firefly luciferase plasmid were a gift from Andrei Seluanov (Vera Gorbunova) from the University of Rochester. In total, 10^6 cells were transfected with 5 µg of firefly reporter plasmid and 0.1 µg of Renilla luciferase via electroporation using the Neon™ Transfection System (MPK1096, Invitrogen) (1100 V, 20 ms and two pulses). Cells were cultured in a 96-well plate (5×10^4 cells/well in 100 µl) overnight in OptiMEM (31,985,070, Gibco; antibiotic free medium). To analyse the transfected cells, a Dual-Luciferase assay kit (E2920 Promega) was used. The luminescence was measured and the ratio of firefly to Renilla was used as an indicator of translational fidelity.

Plasmids	Backbone	Promoter	Mutation
Firefly luciferase	pGL3	SV40	
Firefly luciferase	pGL3	SV40	K529N
HPRT	pGL3	SV40	
Renilla luciferase	pGL3	SV40	

5.11. mHTT immunohistochemistry

Formalin-fixed paraffin-embedded human brains were sectioned sagitally at a 5 µm thickness. For staining, the paraffin was melted at 60 °C for 30 min and solved twice in xylene for 5 min. For rehydration, the slides were placed in a descending alcohol series followed by incubation in running tap water for 30 min. For antigen unmasking, the slides were incubated for 15 min in heated Antigen retrieval solution (DAKO). Following washing, the sections were permeabilised with 0.1 % Triton X. Unspecific endogenous alkaline phosphatase activity was blocked using BLOXALL (Vector laboratories, SP-6000-100) for 10 min. Unspecific antibody binding was blocked using 5 % bovine serum albumin for 30 min. Subsequently, the slides were incubated with 1:120 a-HTT antibody (EM48, Merck Millipore), preferentially detecting mHTT aggregates, overnight at 4 °C in a humid chamber. After washing three times for 5 min in PBS, the slides were incubated with anti-goat biotinylated secondary antibody in a dilution of 1:50 for 30 min at room temperature. The slides were washed and incubated with ABC-HRP mix (Vector laboratories, AK-5100), prepared in advance for 30 min at room temperature. After soaking for 5 min in PBS, the slides were incubated with diaminobenzidine (Vector laboratories) prepared according to the manufacturer's instructions. Development was performed under microscopic control. The slides were washed for 10 min in running tap water and counterstained with haemalaun for 1 min. The slides were washed and dehydrated in an ascending alcohol series, mounted in Eukitt and analysed blinded under the microscope.

5.12. RNA isolation and cDNA synthesis

RNA isolation was performed using the RNeasy Mini Kit (Qiagen). In total, 350 µl RLT buffer and 350 µl ethanol (70 %) were added to the cell pellet and transferred onto a spin column. Following centrifugation at 8000 *g* for 30 s, the flow-through was discarded and 700 µl RWI buffer was added and centrifuged. Subsequently, 500 µl RPE Buffer were added and centrifuged at 8000 *g* for 30 s. The columns were air dried, transferred to new 1.5 ml tubes and 30 µl RNase-free water was added to the column. Following centrifugation, the concentration of the purified RNA was determined via Nanodrop.

A total of 1 µg of RNA was pre-incubated with 250 ng of random hexamer primer $p(dN)_6$ in nuclease-free water for 5 min at 70 °C.The cDNA reaction mix was: 4 µl 5× M-MLV reverse transcriptase buffer, 1 µl M-MLV (400 U/µl) (Promega) and 0.5 µl RNasin (40 U/µl) (Promega) and supplemented with nuclease-free water to 20 µl. Reverse transcription was performed for 1 h at 37 °C. Primers used for qPCR were synthesised after O'Sullivan et al. (O'Sullivan et al., 2002).

5.13. ChIP

For ChIP analysis, 80 % confluent cells were fixed with 1 % formaldehyde at room temperature for 10 min and 0.125 M glycine was used to stop the cross-linking reaction. Cells were washed with PBS, harvested and lysed with ChIP cell lysis buffer on ice for 10 min. Pelleted chromatin was sonicated in ChIP sonicate buffer using a Focused-ultrasonicator (Covaris M220, 1 ml) to yield chromatin fragments with an average size of 600 bp. For chromatin precipitation, Protein A agarose beads or Protein A magnetic dynabeads were used. After incubating 10 µg chromatin with antibodies at 4 °C overnight in IP diluent, chromatin-antibody complexes were washed first with low salt buffer followed by high-salt buffer, LiCl buffer and twice with TE buffer. ChIPed DNA was eluted from beads in µChIP elution buffer for 2 h at 60 °C with 900 rpm. ChIPed DNA was purified using the QIAquick® Nucleotide Removal Kit (28,306, Qiagen) according to the manufacturer's protocol. Samples were qualitatively and quantitatively analysed by PCR and qPCR, respectively. For qualitative ChIP analysis, samples were loaded on a 1 % agarose gel and visualised using the Ged-Doc-It Imager (UVP). For rDNA analysis, primers spanning the complete gene according to O'Sullivan et al. (O'Sullivan et al., 2002) were used.

ChIP cell lysis buffer	5 mM HEPES pH 8.0, 85 mM KCl, 0.5 % NP-40, 1:50 complete
ChIP sonicate buffer	50 mM HEPES pH 7.9, 140 M NaCl, 1 mM EDTA, 1 % Triton X 100, 0.1 % Na-deoxychlorate, 0.1 % SDS, 0.5 mM PMSF, 1:50 complete
µChIP elution buffer	10 mM Tris-Cl pH 8, 1 mM EDTA pH 8, 1 % SDS, 1 % proteinase K
TE buffer	10 mM Tris pH 8, 1 mM EDTA
Protein A agarose beads	Pierce™, Thermofisher Scientific, Waltham, Massachusetts, USA, 20334
Protein A magnetic dynabeads	Invitrogen, Thermofisher Scientific, Waltham, Massachusetts, USA, 10002D
IP diluent	0.1 % SDS, 1 % Triton X 100, 1 mM EDTA pH 8.0, 16.7 mM TrisHCl pH 8.0, 167 mM NaCl, 1:50 complete
Low salt buffer	0.1 % SDS, 1 % Triton X 100, 2 mM EDTA, 20 mM Tris-Cl, pH 8.1, 150 mM NaCl
High-salt buffer	0.1 % SDS, 1 % Triton X 100, 2 mM EDTA, 20 mM Tris-Cl, pH 8.1, 500 mM NaCl
LiCl buffer	10 mM Tris-Cl pH 8.0, 250 mM LiCl, 1 % NP40, 1 % deoxychloric acid, 1 mM EDTA
TE buffer	10 mM Tris pH 8, 1 mM EDTA

5.14. Statistics

All -omics-related analyses of significance levels used a *p*-value cut-off of 0.05, unless specified otherwise. The GSEA cut-off was 0.05 and 0.25 for the p-value and FDR, respectively. The cell biological experiments were proof-of-concept experiments and were performed with at least three independent replicates. Statistical significance was calculated using either one-way student's *t*-test if applicable or one-way analysis of variance with Bonferroni post hoc test after testing for normality and identification of outliers. Results were assumed to be statistically significant with $p < 0.05$.

Ethics approval and consent to participate Ethical approval

Human cell lines from patients with HD and healthy controls were obtained from the EHDN under the EHDN REGISTRY study (Orth et al., 2011). All materials provided by the EHDN repository were obtained after informed written consent according to the International Conference on Harmonisation-Good Clinical Practice guidelines, and the study was conducted in accordance with the Declaration of Helsinki and following approval of the study by the respective institutional ethics committees of the different institutions. The analysis of human post-mortem specimen was covered by a vote of the ethical committee of Ulm University (252/23).

Animal experiments

The studies with animal tissues comply with the current laws in Germany and are covered by a proposal (TVA1553).

Funding

This work was supported by the European Huntington's Disease Network EHDN by a seed fund (1058) to S.I. F.K. and T.P. were members of the graduate programme CEMMA (cellular and molecular mechanisms in ageing), funded by the German Research Foundation DFG. S.I. was supported by a grant of the DFG IB83 3–4. M.M. and S.I. are part of the Collaborative Research Centre CRC1506 “Aging at Interfaces” that is funded by the DFG.

CRediT authorship contribution statement

Maximilian Wagner: Writing – original draft, Visualization, Investigation, Conceptualization. **Gaojie Zhu:** Investigation. **Fatima Khalid:** Investigation. **Tamara Phan:** Investigation. **Pallab Maity:** Investigation, Formal analysis. **Ludmila Lupu:** Investigation. **Eric Agyeman-Duah:** Investigation. **Sebastian Wiese:** Investigation. **Katrin S. Lindenberg:** Supervision, Resources. **Michael Schön:** Resources. **G. Bernhard Landwehrmeyer:** Writing – review & editing, Supervision, Formal analysis. **Marianna Penzo:** Writing – review & editing, Investigation. **Stefan Kochanek:** Supervision, Resources. **Karin Scharffetter-Kochanek:** Writing – review & editing, Supervision, Resources, Formal analysis. **Medhanie Mulaw:** Writing – review & editing, Validation, Supervision, Software, Methodology, Investigation, Formal analysis, Conceptualization. **Sebastian Iben:** Writing – review & editing, Validation, Supervision, Project administration, Funding acquisition, Formal analysis, Conceptualization.

Declaration of competing interest

G.B.L. has provided consulting services, advisory board functions, clinical trial services and/or lectures for Acadia Pharmaceuticals, Affiris, Allergan, Alnylam, Amarin, AOP Orphan Pharmaceuticals AG, Bayer Pharma AG, Boehringer-Ingelheim, CHDI-Foundation, Deutsche Huntington-Hilfe, Desitin, Genentech, Genzyme, GlaxoSmithKline, F. Hoffmann-LaRoche, Ipsen, ISIS Pharma (IONIS), Lilly, Lundbeck, Medesis, Medivation, Medtronic, NeuraMetrix, Neurosearch Inc., Novartis, Pfizer, Prana Biotechnology, Prilenia, PTC Therapeutics, Raptor, Remix Therapeutics, Rhône-Poulenc Rorer, Roche Pharma AG Deutschland, Sage Therapeutics, Sanofi-Aventis, Sangamo/Shire, Siena Biotech, Takeda, Temmler Pharma GmbH, Teva, Triplet Therapeutics, Trophos, UniQure and Wave Life Sciences. The other authors declare no conflict of interests.

Data availability

All data generated or analysed during this study are included in this published article [and its Supplementary files].

Acknowledgements

We want to thank Adelheid Hainzl and Franziska Hoschek for their technical support with IHC and western blot analysis.

Appendix A. Supplementary data

Supplementary data to this article can be found online at https://doi.org/10.1016/j.nbd.2024.106668.

References

Abadi, Martín, Agarwal, Ashish, Barham, Paul, Brevdo, Eugene, Chen, Zhifeng, Citro, Craig, Corrado, Greg S., et al., 2016. TensorFlow: Large-Scale Machine Learning on Heterogeneous Distributed Systems. arXiv. https://doi.org/10.48550/ARXIV.1603.04467.

Alupei, Marius Costel, Maity, Pallab, Esser, Philipp Ralf, Krikki, Ioanna, Tuorto, Francesca, Parlato, Rosanna, Penzo, Marianna, et al., 2018. Loss of Proteostasis is a Pathomechanism in Cockayne syndrome. Cell Rep. 23 (6), 1612–1619. https://doi.org/10.1016/j.celrep.2018.04.041.

Arneson, Douglas, Zhang, Yong, Yang, Xia, Narayanan, Manikandan, 2018. Shared mechanisms among neurodegenerative diseases: from genetic factors to gene networks. J. Genet. 97 (3), 795–806.

Azpurua, Jorge, Ke, Zhonghe, Chen, Iris X., Zhang, Quanwei, Ermolenko, Dmitri N., Zhang, Zhengdong D., Gorbunova, Vera, Seluanov, Andrei, 2013. Naked mole-rat has increased translational Fidelity compared with the mouse, as well as a unique 28S ribosomal RNA cleavage. Proc. Natl. Acad. Sci. USA 110 (43), 17350–17355. https://doi.org/10.1073/pnas.1313473110.

Back, Sung Hoon, 2020. Roles of the translation initiation factor eIF2α phosphorylation in cell structure and function. Cell Struct. Funct. 45 (1), 65–76. https://doi.org/10.1247/csf.20013.

Ballesteros, M., Fredriksson, A., Henriksson, J., Nyström, T., 2001. Bacterial senescence: protein oxidation in non-proliferating cells is dictated by the accuracy of the ribosomes. EMBO J. 20 (18), 5280–5289. https://doi.org/10.1093/emboj/20.18.5280.

Bates, Gillian P., Dorsey, Ray, Gusella, James F., Hayden, Michael R., Kay, Chris, Leavitt, Blair R., Nance, Martha, et al., 2015. Huntington Disease. Nat. Rev. Dis. Primers 1 (April), 15005. https://doi.org/10.1038/nrdp.2015.5.

Benn, C.L., Sun, T., Sadri-Vakili, G., McFarland, K.N., DiRocco, D.P., Yohrling, G.J., Clark, T.W., Bouzou, B., Cha, J.-H.J., 2008. Huntingtin modulates transcription, occupies gene promoters in vivo, and binds directly to DNA in a Polyglutamine-dependent manner. J. Neurosci. 28 (42), 10720–10733. https://doi.org/10.1523/JNEUROSCI.2126-08.2008.

Bradsher, John, Auriol, Jerome, Proietti, Luca, de Santis, Sebastian, Iben, Jean Luc, Vonesch, Ingrid Grummt, Egly, Jean Marc, 2002. CSB is a component of RNA pol I transcription. Mol. Cell 10 (4), 819–829. https://doi.org/10.1016/s1097-2765(02)00678-0.

Brooks, P.J., 2013. Blinded by the UV light: how the focus on transcription-coupled NER has distracted from understanding the mechanisms of Cockayne syndrome neurologic Disease. DNA Repair 12 (8), 656–671. https://doi.org/10.1016/j.dnarep.2013.04.018.

Dukan, S., Farewell, A., Ballesteros, M., Taddei, F., Radman, M., Nyström, T., 2000. Protein oxidation in response to increased transcriptional or translational errors. Proc. Natl. Acad. Sci. USA 97 (11), 5746–5749. https://doi.org/10.1073/pnas.100422497.

Eshraghi, Mehdi, Karunadharma, Pabalu P., Blin, Juliana, Shahani, Neelam, Ricci, Emiliano P., Michel, Audrey, Urban, Nicolai T., et al., 2021. Mutant huntingtin stalls ribosomes and represses protein synthesis in a cellular model of Huntington Disease. Nat. Commun. 12 (1), 1461. https://doi.org/10.1038/s41467-021-21637-y.

Gidalevitz, Tali, Ben-Zvi, Anat, Ho, Kim H., Brignull, Heather R., Morimoto, Richard I., 2006. Progressive Disruption of Cellular Protein Folding in Models of Polyglutamine Diseases. Science (New York, N.Y.) 311 (5766), 1471–1474. https://doi.org/10.1126/science.1124514.

Huang, Bin, Lucas, Tanja, Kueppers, Claudia, Dong, Xiaomin, Krause, Maike, Bepperling, Alexander, Buchner, Johannes, et al., 2015. Scalable production in human cells and biochemical characterization of full-length Normal and mutant huntingtin. PLoS One 10 (3), e0121055. https://doi.org/10.1371/journal.pone.0121055.

Iben, Sebastian, Tschochner, Herbert, Bier, Mirko, Hoogstraten, Deborah, Hozák, Pavel, Egly, Jean Marc, Grummt, Ingrid, 2002. TFIIH plays an essential role in RNA polymerase I transcription. Cell 109 (3), 297–306. https://doi.org/10.1016/s0092-8674(02)00729-8.

Jurcau, Anamaria, 2022. Molecular pathophysiological mechanisms in Huntington's Disease. Biomedicines 10 (6), 1432. https://doi.org/10.3390/biomedicines10061432.

Karikkineth, Ajoy C., Scheibye-Knudsen, Morten, Fivenson, Elayne, Croteau, Deborah L., Bohr, Vilhelm A., 2017. Cockayne syndrome: clinical features, model systems and pathways. Ageing Res. Rev. 33 (January), 3–17. https://doi.org/10.1016/j.arr.2016.08.002.

Kennedy, L., 2003. Dramatic tissue-specific mutation length increases are an early molecular event in Huntington Disease pathogenesis. Hum. Mol. Genet. 12 (24), 3359–3367. https://doi.org/10.1093/hmg/ddg352.

Koch, Sylvia, Gonzalez, Omar Garcia, Assfalg, Robin, Schelling, Adrian, Schäfer, Patrick, Scharffetter-Kochanek, Karin, Iben, Sebastian, 2014. Cockayne syndrome protein a is a transcription factor of RNA polymerase I and stimulates ribosomal biogenesis and growth. Cell Cycle (Georgetown, Tex.) 13 (13), 2029–2037. https://doi.org/10.4161/cc.29018.

Labadorf, Adam, Hoss, Andrew G., Lagomarsino, Valentina, Latourelle, Jeanne C., Hadzi, Tiffany C., Bregu, Joli, MacDonald, Marcy E., et al., 2015. RNA sequence analysis of human Huntington Disease brain reveals an extensive increase in inflammatory and developmental gene expression. PLoS One 10 (12), e0143563. https://doi.org/10.1371/journal.pone.0143563.

Landwehrmeyer, G.B., McNeil, S.M., Dure, L.S., Ge, P., Aizawa, H., Huang, Q., Ambrose, C.M., Duyao, M.P., Bird, E.D., Bonilla, E., 1995. Huntington's Disease gene: regional and cellular expression in brain of Normal and affected individuals. Ann. Neurol. 37 (2), 218–230. https://doi.org/10.1002/ana.410370213.

Lanzafame, Manuela, Branca, Giulia, Landi, Claudia, Qiang, Mingyue, Vaz, Bruno, Nardo, Tiziana, Ferri, Debora, et al., 2021. Cockayne syndrome group a and Ferrochelatase finely tune ribosomal gene transcription and its response to UV irradiation. Nucleic Acids Res. 49 (19), 10911–10930. https://doi.org/10.1093/nar/gkab819.

Laugel, Vincent, 1993. Cockayne syndrome. In: Adam, Margaret P., Feldman, Jerry, Mirzaa, Ghayda M., Pagon, Roberta A., Wallace, Stephanie E., Bean, Lora J.H., Gripp, Karen W., Amemiya, Anne (Eds.), GeneReviews®. University of Washington, Seattle, Seattle (WA). http://www.ncbi.nlm.nih.gov/books/NBK1342/.

Lebedev, Anton, Scharffetter-Kochanek, Karin, Iben, Sebastian, 2008. Truncated Cockayne syndrome B protein represses elongation by RNA polymerase I. J. Mol. Biol. 382 (2), 266–274. https://doi.org/10.1016/j.jmb.2008.07.018.

Lee, Jong-Min, Correia, Kevin, Loupe, Jacob, Kim, Kyung-Hee, Barker, Douglas, Hong, Eun Pyo, Chao, Michael J., et al., 2019. CAG repeat not Polyglutamine length determines timing of Huntington's Disease onset. Cell 178 (4), 887–900.e14. https://doi.org/10.1016/j.cell.2019.06.036.

Levin, P.S., Green, W.R., Victor, D.I., MacLean, A.L., 1983. Histopathology of the Eye in Cockayne's Syndrome. Arch. Ophthalmol. (Chicago, Ill.: 1960) 101 (7), 1093–1097. https://doi.org/10.1001/archopht.1983.01040020095016.

Li, S.H., Schilling, G., Young, W.S., Li, X.J., Margolis, R.L., Stine, O.C., Wagster, M.V., Abbott, M.H., Franz, M.L., Ranen, N.G., 1993. Huntington's Disease gene (IT15) is widely expressed in human and rat tissues. Neuron 11 (5), 985–993. https://doi.org/10.1016/0896-6273(93)90127-d.

Liang, Fangkeng, Li, Bijuan, Yingying, Xu, Gong, Junwei, Zheng, Shaohui, Zhang, Yunlong, Wang, Yuming, 2023. Identification and characterization of Necdin as a target for the Cockayne syndrome B protein in promoting neuronal differentiation and maintenance. Pharmacol. Res. 187 (January), 106637 https://doi.org/10.1016/j.phrs.2022.106637.

Miller, James R.C., Lo, Kitty K., Andre, Ralph, Hensman, Davina J., Moss, Ulrike Träger, Stone, Timothy C., Jones, Lesley, Holmans, Peter, Plagnol, Vincent, Tabrizi, Sarah J., 2016. RNA-Seq of Huntington's Disease patient myeloid cells reveals innate transcriptional dysregulation associated with Proinflammatory pathway activation. Hum. Mol. Genet. 25 (14), 2893–2904. https://doi.org/10.1093/hmg/ddw142.

Mootha, Vamsi K., Lindgren, Cecilia M., Eriksson, Karl-Fredrik, Subramanian, Aravind, Sihag, Smita, Lehar, Joseph, Puigserver, Pere, et al., 2003. PGC-1alpha-responsive genes involved in oxidative phosphorylation are coordinately downregulated in human diabetes. Nat. Genet. 34 (3), 267–273. https://doi.org/10.1038/ng1180.

Mukherjee, Shradha, Klaus, Christine, Pricop-Jeckstadt, Mihaela, Miller, Jeremy A., Struebing, Felix L., 2019. A microglial signature directing human aging and neurodegeneration-related gene networks. Front. Neurosci. 13, 2. https://doi.org/10.3389/fnins.2019.00002.

Noori, Ayush, Mezlini, Aziz M., Hyman, Bradley T., Serrano-Pozo, Alberto, Das, Sudeshna, 2021a. Differential gene expression data from the human central nervous system across Alzheimer's Disease, Lewy body diseases, and the amyotrophic lateral sclerosis and frontotemporal dementia Spectrum. Data Brief 35 (April), 106863. https://doi.org/10.1016/j.dib.2021.106863.

Noori, Ayush, Mezlini, Aziz M., Hyman, Bradley T., Serrano-Pozo, Alberto, Das, Sudeshna, 2021b. Systematic review and Meta-analysis of human transcriptomics reveals Neuroinflammation, deficient energy metabolism, and Proteostasis failure across neurodegeneration. Neurobiol. Dis. 149 (February), 105225 https://doi.org/10.1016/j.nbd.2020.105225.

Nyström, Thomas, 2005. Role of oxidative Carbonylation in protein quality control and senescence. EMBO J. 24 (7), 1311–1317. https://doi.org/10.1038/sj.emboj.7600599.

Okur, Mustafa N., Fang, Evandro F., Fivenson, Elayne M., Tiwari, Vinod, Croteau, Deborah L., Bohr, Vilhelm A., 2020. Cockayne syndrome proteins CSA and CSB maintain mitochondrial homeostasis through NAD+ signaling. Aging Cell 19 (12), e13268. https://doi.org/10.1111/acel.13268.

Orth, Michael, European Huntington's Disease Network, Handley, O.J., Schwenke, C., Dunnett, S., Wild, E.J., Tabrizi, S.J., Landwehrmeyer, G.B., 2011. Observing Huntington's Disease: the European Huntington's Disease Network's REGISTRY. J. Neurol. Neurosurg. Psychiatry 82 (12), 1409–1412. https://doi.org/10.1136/jnnp.2010.209668.

O'Sullivan, Audrey C., Sullivan, Gareth J., McStay, Brian, 2002. UBF binding in vivo is not restricted to regulatory sequences within the vertebrate ribosomal DNA repeat. Mol. Cell. Biol. 22 (2), 657–668. https://doi.org/10.1128/MCB.22.2.657-668.2002.

Pressl, Christina, Mätlik, Kert, Kus, Laura, Darnell, Paul, Luo, Ji-Dung, Paul, Matthew R., Weiss, Alison R., et al., 2024. Selective vulnerability of layer 5a Corticostriatal neurons in Huntington's Disease. Neuron 112 (6), 924–941.e10. https://doi.org/10.1016/j.neuron.2023.12.009.

Qiang, Mingyue, Khalid, Fatima, Phan, Tamara, Ludwig, Christina, Scharffetter-Kochanek, Karin, Iben, Sebastian, 2021. Cockayne syndrome-associated CSA and CSB mutations impair ribosome biogenesis, ribosomal protein stability, and global protein folding. Cells 10 (7), 1616. https://doi.org/10.3390/cells10071616.

Ritchie, Matthew E., Phipson, Belinda, Di, Wu, Yifang, Hu, Law, Charity W., Shi, Wei, Smyth, Gordon K., 2015. Limma powers differential expression analyses for RNA-sequencing and microarray studies. Nucleic Acids Res. 43 (7), e47 https://doi.org/10.1093/nar/gkv007.

Sagar, Vidya, Pilakka-Kanthikeel, S., Martinez, Paola C., Atluri, V.S.R., Nair, M., 2017. Common gene-Network signature of different neurological disorders and their potential implications to neuroAIDS. PLoS One 12 (8), e0181642. https://doi.org/10.1371/journal.pone.0181642.

Sönmez, Aynur, Mustafa, Rasem, Ryll, Salome T., Tuorto, Francesca, Wacheul, Ludivine, Ponti, Donatella, Litke, Christian, et al., 2021. Nucleolar stress controls mutant Huntington toxicity and monitors Huntington's Disease progression. Cell Death Dis. 12 (12), 1139. https://doi.org/10.1038/s41419-021-04432-x.

Strong, T.V., Tagle, D.A., Valdes, J.M., Elmer, L.W., Boehm, K., Swaroop, M., Kaatz, K.W., Collins, F.S., Albin, R.L., 1993. Widespread expression of the human and rat Huntington's Disease gene in brain and nonneural tissues. Nat. Genet. 5 (3), 259–265. https://doi.org/10.1038/ng1193-259.

Subramanian, Aravind, Tamayo, Pablo, Mootha, Vamsi K., Mukherjee, Sayan, Ebert, Benjamin L., Gillette, Michael A., Paulovich, Amanda, et al., 2005. Gene set enrichment analysis: a knowledge-based approach for interpreting genome-wide expression profiles. Proc. Natl. Acad. Sci. USA 102 (43), 15545–15550. https://doi.org/10.1073/pnas.0506580102.

Tabrizi, Sarah J., Flower, Michael D., Ross, Christopher A., Wild, Edward J., 2020. Huntington Disease: new insights into molecular pathogenesis and therapeutic opportunities. Nat. Rev. Neurol. 16 (10), 529–546. https://doi.org/10.1038/s41582-020-0389-4.

Tahmasebi, Soroush, Khoutorsky, Arkady, Mathews, Michael B., Sonenberg, Nahum, 2018. Translation deregulation in human Disease. Nat. Rev. Mol. Cell Biol. 19 (12), 791–807. https://doi.org/10.1038/s41580-018-0034-x.

Team RC, 2015. R: A Language and Environment for Statistical Computing.

Thomas, Paul D., Kejariwal, Anish, Campbell, Michael J., Mi, Huaiyu, Diemer, Karen, Guo, Nan, Ladunga, Istvan, et al., 2003. PANTHER: a Browsable database of gene products organized by biological function, using curated protein family and subfamily classification. Nucleic Acids Res. 31 (1), 334–341. https://doi.org/10.1093/nar/gkg115.

Treaster, S.B., Ridgway, I.D., Richardson, C.A., Gaspar, M.B., Chaudhuri, A.R., Austad, S. N., 2014. Superior proteome stability in the longest lived animal. Age (Dordr.) 36 (3), 9597. https://doi.org/10.1007/s11357-013-9597-9.

Vessoni, Alexandre T., Herai, Roberto H., Karpiak, Jerome V., Leal, Angelica M.S., Trujillo, Cleber A., Quinet, Annabel, Agnez, Lucymara F., Lima, Carlos F.M., Menck, and Alysson R. Muotri., 2016. Cockayne syndrome-derived neurons display reduced synapse density and altered neural Network synchrony. Hum. Mol. Genet. 25 (7), 1271–1280. https://doi.org/10.1093/hmg/ddw008.

Wang, Yuming, Chakravarty, Probir, Ranes, Michael, Kelly, Gavin, Brooks, Philip J., Neilan, Edward, Stewart, Aengus, Schiavo, Giampietro, Svejstrup, Jesper Q., 2014. Dysregulation of gene expression as a cause of Cockayne syndrome neurological Disease. Proc. Natl. Acad. Sci. USA 111 (40), 14454–14459. https://doi.org/10.1073/pnas.1412569111.